CFD modelling of hydrogen and hydrogen-methane explosions – Analysis of varying concentration and reduced oxygen atmospheres

Melodia Lucas [a,b,*], Helene Hisken [a,b], Trygve Skjold [b], Bjørn J. Arntzen [a,b], Kees van Wingerden [c]

[a] Gexcon, Bergen, Norway
[b] Department of Physics and Technology, University of Bergen, Bergen, Norway
[c] Vysus Group, Bergen, Norway

A B S T R A C T

This paper evaluates the predictive capabilities of the advanced consequence model FLACS-CFD for deflagrations involving hydrogen. Two modelling approaches are presented: the extensively validated model system originally developed for hydrocarbons included in FLACS-CFD *22.1* and a Markstein number dependent model implemented in the in-house version FLACS-CFD *22.1 IH*. The ability of the models to predict the overpressure and the flame arrival time for scenarios with different concentrations of hydrogen, and thus different Lewis and Markstein numbers, is assessed. Furthermore, the effect of adding methane or nitrogen on overpressure for different regimes of premixed combustion are investigated. The validation dataset includes deflagrations in the open or in congested open areas and vented deflagrations in empty or congested enclosures. The overpressure predictions by FLACS-CFD *22.1 IH* are found to be more accurate than those obtained with FLACS-CFD *22.1* for scenarios with varying hydrogen concentrations and/or added nitrogen or methane in the mixture. The predictions by FLACS-CFD *22.1 IH* for lean hydrogen mixtures are within a factor of 2 of the values observed in the experiments. Further development of the model is needed for more accurate prediction of deflagrations involving rich hydrogen mixtures as well as scenarios with other fuels and/or conditions where the initial pressure or temperature deviate significantly from ambient conditions.

1. Introduction

If used within their validated range of applicability, consequence models can be valuable tools for investigating the effects of various explosion protection measures as well as for optimising the design of systems where hydrogen is produced, transported, and used. Relevant examples are installations for hydrogen production by electrolysis, fuel-cell stacks in ships, and pipeline networks previously used for distribution of natural gas. Meanwhile, hydrogen is the most reactive and easily ignitable of all energy carriers ever considered for widespread use in society, and the propensity of hydrogen-air mixtures to undergo deflagration-to-detonation-transition has severe implications for explosion protection and safety distances (Skjold, 2020). The high reactivity of hydrogen-air mixtures implies that minor inaccuracies in engineering models, mainly developed for and validated against explosion scenarios involving conventional fuels, can have an unacceptable impact on the model's capability of representing hydrogen-related accidents. This implies that quantifying the uncertainty associated with model

predictions for hydrogen applications potentially can be more challenging compared to applications involving hydrocarbons. For example, the results from the second HySEA blind-prediction study showed that the spread in predicted maximum overpressures from seven different modellers, using four different computational fluid dynamics (CFD) models for the same scenario, covered two orders of magnitude (Skjold et al., 2019).

The FLACS-Hydrogen module in FLACS-CFD has been developed to represent accident scenarios involving hydrogen through several research programmes and projects over the last two decades. Middha (2010) carried out extensive validation studies for hydrogen dispersion and explosion scenarios, including the participation in several blind-prediction benchmark studies. Most of the hydrogen explosion validation work presented in Middha (2010) was done as part of the Network of Excellence HySafe (NoE HySafe). The validation work included experiments in a tube with different obstacle configurations (Breitung et al., 2005; Middha et al., 2007), in a mockup refuelling station (Makarov et al., 2009), in unconfined explosion scenarios with

various degrees of congestion (Royle et al., 2007) and in a one-fifth scale model of a traffic tunnel (Sato et al., 2006). Hisken (2018) implemented and validated new sub-grid models in an in-house development version of FLACS. Lucas et al. (2021) validated this model version against the combined dispersion and explosion experiments performed as part of the HySEA project. The performance of the new model was significantly improved compared to the latest release version at the time (FLACS v10.9) for those experiments. However, an extensive validation study for different fuels and scenarios showed worse representation of the experimental results for some experimental campaigns representing full-scale scenarios. FLACS-CFD is used to simulate actual accident scenarios in industry, and it is possible to include many chemical components. Thus, new models need to be general enough to simulate the complex geometries encountered for systems on industrial scale and represent different initial conditions. This paper analyses the performance of two modelling frameworks for premixed combustion in FLACS-CFD: FLACS-CFD *22.1* and FLACS-CFD *22.1 IH*. FLACS-CFD *22.1* is a commercial version of FLACS-CFD released in 2022, while FLACS-CFD *22.1 IH* is an in-house development version that replaces the burning velocity correlations in FLACS-CFD *22.1* with the Markstein number dependent combustion model implemented by Hisken (2018). The aim of this work is to investigate the predictive capabilities of the tool for scenarios with various equivalence ratios (ER), blends of hydrogen and other fuels, and flame propagation in non-standard atmospheres. The findings will inform the further development of the model.

2. Modelling

FLACS-CFD is an advanced numerical model system for assessing the consequences of accidental releases, dispersion, fires and explosions in complex geometries. FLACS-Hydrogen is a submodule of the general CFD tool, developed for pure hydrogen or blends of hydrogen with other fuels such as methane. The Favre-averaged Navier-Stokes equations are solved on a cartesian grid. The k-ε turbulence model is used (Launder and Spalding, 1974). The Discrete Transfer Method (DTM) (Muthusamy et al., 2011) model is used to model radiation losses to the surroundings. The combustion model includes sub-models for the burning velocity, flame folding downstream of obstacles, and the integral length scale. Further details about the standard models used in FLACS-CFD can be found in the User's Manual (Gexcon et al., 2022). The differences between FLACS-CFD *22.1* and FLACS-CFD *22.1 IH* are limited to the burning velocity models. In the following, the two different approaches for computing the burning velocity are described in detail.

The laminar burning velocity, s_L, in FLACS-CFD is tabulated for different fuels and equivalence ratios. For hydrogen, the data is taken from an experimental study by Taylor (1991) with s_L obtained from outwardly propagating spherical flames. For fuel blends, a mixture rule based on the number of moles of oxygen needed for complete combustion is used. For modelling the cellular flame propagation, a quasi-laminar burning velocity correlation is used. For hydrogen explosions, the transition from laminar to cellular flame propagation occur shortly after ignition. The quasi-laminar burning velocity model dominates for uncongested scenarios where the turbulence level is low. The empirical model for the quasi-laminar burning velocity, s_{QL}, in FLACS-CFD reads

$$s_{QL} = s_{L,Le}\left(1 + C_{QL}\left(min\left[1, \frac{r_F}{3}\right]\right)^a\right). \tag{1}$$

Here $s_{L,Le}$ is the laminar burning velocity corrected for thermal-diffusive instabilities, r_F is the flame radius, $a = 0.5$ and C_{QL} is a mixture dependent constant. For hydrogen $C_{QL} = 3.5$ and for methane $C_{QL} = 1.6$, for blends a mixture fraction rule is used. In the in-house development version of FLACS-CFD, s_{QL} is modelled as

$$s_{QL} = max\left(s_L, s_L C_{QL}^*\left(\frac{r_F}{r_{F,cr}}\right)^{a^*}\right), \tag{2}$$

where $r_{F,cr}$ denotes the critical radius of the appearance of a cellular flame, and the model constants C_{QL}^* and a^* are both concentration and mixture-dependent. The data from Bauwens et al. (2017a,b) are used for the $r_{F,cr}$, C_{QL}^* and a^* values for hydrogen and methane.

For the turbulent regime, the turbulent burning velocity, s_T, is expressed in terms of the effective root-mean-square turbulence velocity u' and the Karlovitz stretch factor K (Bradley et al., 2013) as

$$\frac{s_T}{u'} = \alpha K^{-\beta}. \tag{3}$$

In FLACS-CFD *22.1*, $\alpha = 0.875$ and $\beta = -0.392$. In FLACS-CFD *22.1 IH*, α and β are empirical parameters explicitly expressed in terms of the strain rate Markstein number, Ma_{sr}. The expressions are based on the correlations given by Bradley et al. (2013) with

$$\alpha = C_a 0.023(30 - Ma_{sr}) \text{ and } \beta = 0.0103(Ma_{sr} - 30) \text{ if } Ma_{sr} > 0 \tag{4}$$

$$\alpha = C_a 0.085(7 - Ma_{sr}) \text{ and } \beta = -0.0075(30 + Ma_{sr}) \text{ if } Ma_{sr} < 0.$$

Here, C_α is a constant model parameter. The Ma_{sr} data by Bradley et al. (2013) is used, where the Ma_{sr} values are determined from the stretched and unstretched flame speeds using extrapolation models. The values are highly dependent on the extrapolation method and the uncertainty is estimated to be about one order of magnitude larger than for the s_L (Han et al., 2020). The Karlovitz stretch factor is expressed as

$$K = C_k \left(\frac{u'}{s_L}\right)^2 \left(\frac{u' l_I}{\nu}\right)^{-0.5}, \tag{5}$$

where $C_k = 0.157$ (Bray, 1990) in FLACS-CFD *22.1* and $C_k = 0.25$ (Bradley et al., 2013) in FLACS-CFD *22.1 IH* and ν is the kinematic viscosity. Then integral length scale, l_I is computed as

$$l_I = min\left(C_{r_F} r_F, C_{l_{lim}} l_{lim}\right), \tag{6}$$

where C_{rF} and C_{llim} are model parameters, and l_{lim} is the distance to the enclosing walls. In FLACS-CFD *22.1*, s_L in Equation (5) includes the Lewis-number correction. The values for the model parameters C_α, C_{rF} and C_{llim} in FLACS-CFD *22.1 IH* are found by peak overpressure and pressure impulse calibration of the solver against selected experimental campaigns (Both et al., 2019).

3. Experiments

This section introduces a collection of experimental campaigns used for validating the burning velocity models. The set-ups of these experiments allow for studying the various submodels of the two combustion model approaches.

3.1. 3D corner small scale

The small scale 3D corner geometry consists of three perpendicular square steel plates of 0.37 m × 0.37 m mounted to form a corner (Renoult and Wilkins, 2004). For the experiments studied here, the obstacle set consisted of four layers of 0.05 m diameter and 0.365 m long pipes (Fig. 1a). The rows of tubes were collocated perpendicularly to each other. The gas used as fuel was either 100 vol% hydrogen or a mixture of 75 vol% hydrogen and 25 vol% nitrogen. The ignition source was mounted on the floor at the inner corner. Four pressure transducers (P1–P4) were mounted at the steel walls. The coordinates in meters from the inner corner of the rig are (0.000, 0.045, 0.047) for P1, (0.000, 0.176, 0.315) for P2, (0.270, 0.000, 0.110) for P3 and (0.350, 0.355, 0.000) for P4.
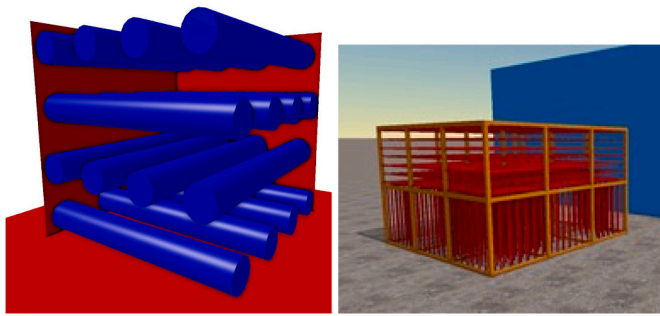
(a) 3D corner small scale.   (b) Repeated pipe congestion.

Fig. 1. Geometry models for the open congested geometries.

3.2. Vented empty enclosure

Bauwens et al. (2012) reported explosion experiments performed by FM Global in an empty chamber with different vent sizes, ignition locations and hydrogen concentrations. The vented chamber was 4.6 m × 4.6 m x 3.0 m. The experiments with the 2.7 m² vent size and centre ignition are used for validation in this paper. The hydrogen concentration varied from 12.1 to 19.7 vol%.

3.3. MOGELEG channel

Renoult and Wilkins (2004) reported laboratory scale experiments performed in a 1.44 m × 0.3 m x 0.3 m rectangular channel. The channel was closed at one end and contained rectangular plates as obstructions. The plates were 0.3 m wide, 0.05 m high and 0.005 m thick. The channel had either two plates located at 0.48 and 0.96 m from the closed end of the channel or four plates at 0.24, 0.48, 0.96 and 1.44 m from the closed end of the channel. The gas used as fuel was either 100 vol% hydrogen or a mixture of 75 vol% hydrogen and 25 vol% nitrogen. The mixtures were ignited near the centre of the closed end of the channel. Pressure transducers were mounted on a sidewall of the channel at 0.06 m from the floor, P1 at 0.135 m, P2 at 0.65 m and P3 at 1.135 m from the end of the channel. Fig. 2 illustrates the four obstacles configuration and the location of the pressure transducers and the ignition source.

3.4. HySEA

Skjold (2018) reported hydrogen deflagrations in 20-foot shipping containers performed as part of the HySEA project at the Gexcon test site outside Bergen, Norway. The tests with venting through the roof and a pipes rack located at the centre of the container are used in this work for validation of the models. Details about the geometry are given by Skjold et al. (2017). The hydrogen concentration was either 21 vol% or 24 vol %. The vent openings on the roof of the container were covered with either commercial panels or plastic sheets and the number was either four, six or eight. The ignition source was located at the centre of the floor. The pressure sensors inside the container were located

symmetrically 0.2 m above the floor of the container and 0.085 m from the sidewalls. P01–P02 were located at 0.58 m, P03–P04 at 2.153 m, P05–P06 at 3.690 m, and P07–P08 at 5.245 m from the back wall of the container.

3.5. Repeated pipe congestion

Hydrogen (Shirvill et al., 2019a) and hydrogen-methane blends (Shirvill et al., 2019b) were ignited in a 3 m × 3 m x 2 m rig with metal bars serving as obstacles at the test site of Health and Safety Executive (HSE) in Buxton. For the hydrogen-methane blends, an equivalence ratio of 1.1 was used. For the hydrogen tests, both lean and rich mixtures were tested. The congestion consisted of vertical and horizontal pipes of about 0.026 m diameter. In the lower part of the rig, 1 m long pipes were located vertically. For the 4-gate congestion type (used for the pure hydrogen tests), four layers of pipes were located around the ignition location. The 9-gate type (used for the hydrogen-methane tests) consisted of nine layers of pipes (Fig. 1b). In the upper part, four layers of pipes were located horizontally for the 4-gate congestion type and seven layers for the 9-gate congestion type.

4. Results and discussion

This section summarizes the results for each experimental campaign. The grid resolution is not varied in this study, since the aim is to compare different burning velocity models. The cells are cubical, and the grid resolution used follow the current guidelines in the FLACS-CFD User's Manual (Gexcon et al., 2022). The time step limit is imposed by the Courant-Friedrichs-Levy (CFL) numbers, with $CFLC = 5$ and $CFLV = 0.5$. The *PLANE WAVE* boundary condition (Gexcon et al., 2022) is used. One scenario for each of the experimental campaigns was simulated with the heat losses model. The maximum difference in peak overpressure was 8.5% for a 3D Corner small scale scenario, for the other scenarios the differences are lower. Due to the relatively small differences and the high computational cost, the heat losses models were not activated for the simulations presented here.

4.1. 3D Corner small scale

Fig. 3 shows the maximum overpressure as a function of ER for the congested unconfined experiments, the 3D corner campaign, for the hydrogen (a) and the hydrogen-nitrogen tests (b). The grid resolution used in the simulations is 0.023 m. The experimental data is filtered using a Savitzky-Golay filter of zero order with a time window of 0.1 ms. The maximum overpressure increases with ER for the pure hydrogen test with ER varying from 0.73 to 1.04 for both experiments and FLACS-CFD *22.1 IH*. FLACS-CFD *22.1* predicts the highest maximum overpressure for the test with ER = 0.9 and decreases with increasing ER. Simulations with both FLACS-CFD versions predict a decrease in maximum overpressure for the test with ER = 1.51 relative to the test with ER = 1.04. Fig. 3b shows the variation of the maximum overpressure with equivalence ratio for the congested unconfined experiments with 75 vol% hydrogen and 25 vol% nitrogen. The maximum overpressure increases
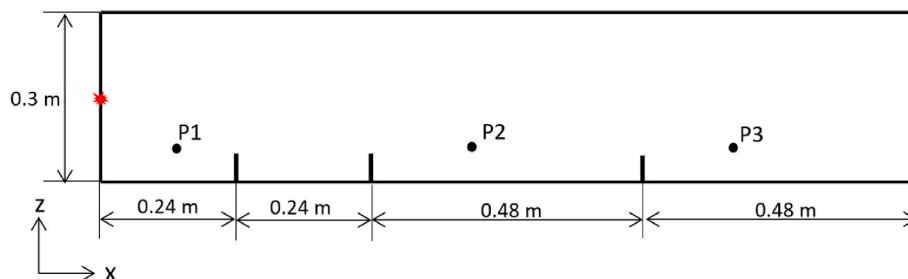

Fig. 2. Sketch of the MOGELEG channel.

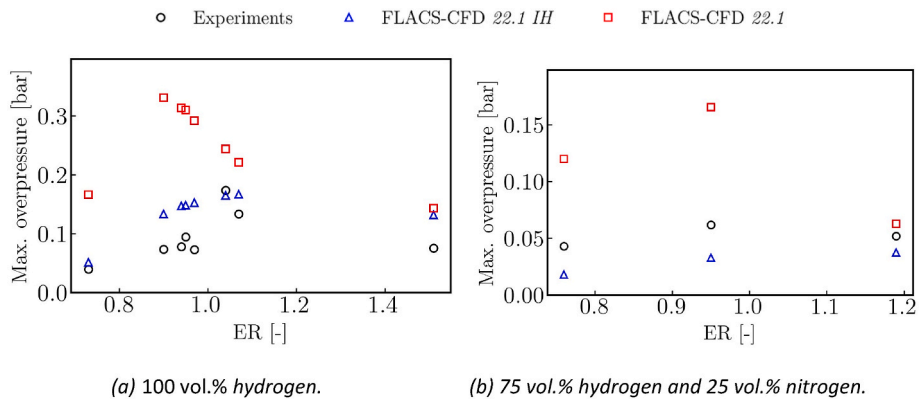*(a) 100 vol.% hydrogen.*   *(b) 75 vol.% hydrogen and 25 vol.% nitrogen.*

Fig. 3. Maximum overpressure with equivalence ratio for the 3D corner experiments.

with the equivalence ratio for the lean hydrogen-nitrogen-air mixtures tested, as for the hydrogen-air mixtures. For a given ER, the addition of nitrogen reduces the maximum overpressure in both experiments and simulations, except for the experiment with the lowest ER tested.

The maximum overpressures occur when the flame reaches the end of the rig. For the lean hydrogen-air mixture tests, the laminar burning velocity in FLACS-CFD *22.1* is higher than in FLACS-CFD *22.1 IH*. The initial flame propagation is driven by the quasi-laminar regime and the flame speed predictions by both FLACS-CFD versions are similar. Once the flame reaches the first rows of obstacles, the turbulent burning regime dominates and FLACS-CFD *22.1* predicts a faster flame propagation, resulting in a higher pressure peak. For the test with ER = 1.51, the laminar burning velocity of FLACS-CFD *22.1 IH* is higher than for FLACS-CFD *22.1*, the computed quasi-laminar burning velocity is also higher, resulting in a faster initial flame propagation and higher turbulence levels. However, the difference in turbulent burning velocity is not significant and the maximum overpressure predicted by FLACS-CFD *22.1* is slightly higher. Fig. 4 shows the range of turbulent burning velocity computed by the models in both versions for $l_C = 2$ mm and 10 mm (on the order of the value predicted for these scenarios) and varying u'. For the ER range in these experiments the turbulent burning velocity computed by FLACS-CFD *22.1* is similar or higher than the one computed by FLACS-CFD *22.1 IH*.

4.2. Vented empty enclosure

Figs. 5 and 6 show the pressure-time curves and flame speed vs distance from ignition for the vented explosion tests in the empty enclosure (Bauwens et al., 2012). The pressure-time curves were filtered using an 80 Hz low pass filter. The grid resolution used in these simulations is 0.1 m. Fig. 5a shows the pressure-time curves for the tests with

a concentration of 18 vol% hydrogen in air. Both FLACS-CFD versions predict two pressure-peaks as observed in the experiments. The increase in overpressure slows down at about 100 ms after ignition in the experiments and after about 150 ms in the predictions by FLACS-CFD *22.1 IH*. When the flame reaches the vent opening, the rate of pressure rise increases and the expelled hydrogen burns outside of the chamber. The first peak occurs when the fuel outside the chamber is burned. The second peak, which is lower than the first peak, occurs when the flame reaches the side walls of the chamber. Fig. 5b shows the flame speed vs distance from ignition for the test with 18 vol% hydrogen-air. The initial flame speed is overpredicted by ±60–80% by FLACS-CFD *22.1* and by ±40–60% by FLACS-CFD *22.1 IH*. The simulated burning velocity inside the chamber is governed by the quasi-laminar regime, while for the external explosion, the turbulent burning velocity governs the flame propagation. The maximum flame speed predictions by FLACS-CFD *22.1* are about 23 m/s higher than the predictions by FLACS-CFD *22.1 IH* and occur outside of the chamber. The first peak, related to the external explosion, is therefore higher for the simulations with FLACS-CFD *22.1*. The flame propagation inside the chamber is also faster in the predictions by FLACS-CFD *22.1* and results in a higher second peak.

The two pressure peaks for the scenario with 19 vol% hydrogen are higher than for the 18 vol% hydrogen scenario. The time between the occurrence of the peaks is also shorter, as expected.

Fig. 7 shows the maximum overpressure, due to the external explosion, with equivalence ratio for the experiments in the empty chamber. The increase in maximum overpressure with the equivalence ratio for the lean hydrogen-air mixtures presented is more pronounced in the simulations than in the experiments. For the highest equivalence ratios considered, the predictions by FLACS-CFD *22.1* are more than two times higher than the maximum overpressure observed in the experiments.
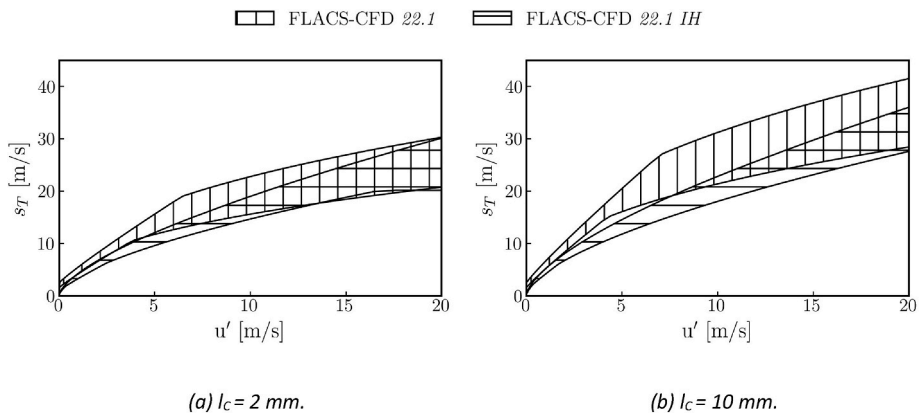

(a) l_C = 2 mm.   *(b) l_C = 10 mm.*

Fig. 4. Turbulent burning velocities as a function of u' for hydrogen-air mixtures with ER in the range [0.6, 1.6].

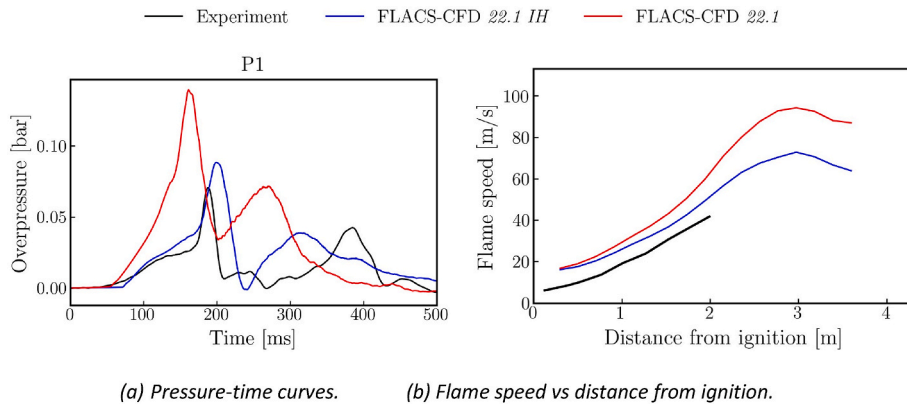*(a) Pressure-time curves.*   *(b) Flame speed vs distance from ignition.*

Fig. 5. Vented empty enclosure test with 18 vol% hydrogen.

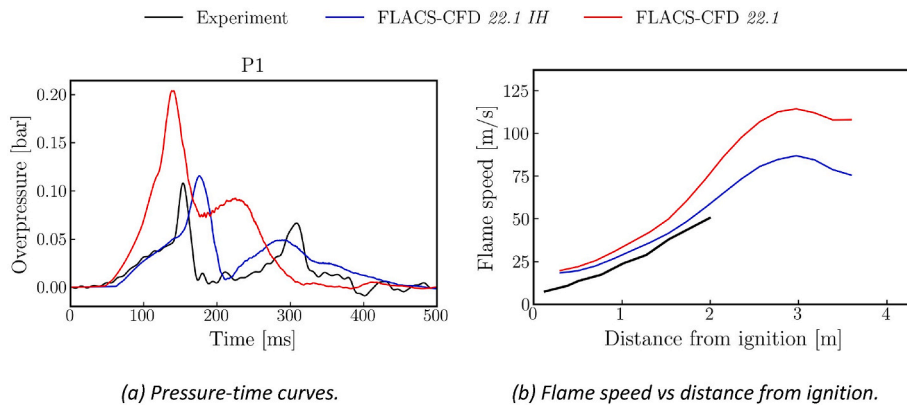*(a) Pressure-time curves.*   *(b) Flame speed vs distance from ignition.*

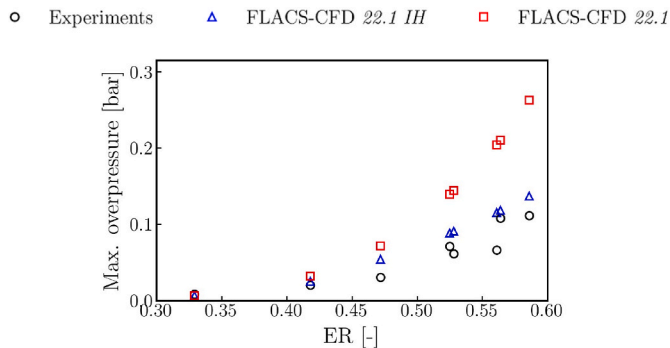**Fig. 6.** Vented empty enclosure with 19 vol% hydrogen.

Fig. 7. Maximum overpressure with ER for the experiments in the vented empty enclosure.

4.3. MOGELEG

Fig. 8 shows the pressure-time curves for Test09 and Test47, and for Test32 and Test34 at the three pressure transducers located in the 1.44 m channel. The pressure-time curves are filtered using a moving average filter with a time window of 0.1 ms. The grid resolution is 0.02 m. Test09 and Test47 were performed in the channel with two obstacles filled with a stoichiometric hydrogen-air mixture. Similar trends were observed for simulations and experiments. The pressure starts to increase at P1, the increase starts earlier for the simulations with FLACS-CFD *22.1 IH* because of higher predictions of s_{QL}, which is dominant before the flame passes the first obstacle. When the unburnt fuel starts being pushed out of the channel, the pressure increase flattens for a short period. After the

flame passes the second obstacle, the turbulent burning regime dominates and FLACS-CFD *22.1* predicts higher overpressures due to higher predictions of s_T. The first peak occurs when the flame reaches the open end of the channel (see Fig. 8). The second peak occurs when the expelled fuel burns outside of the channel. The second peak travels inwards in the channel and is less visible for P3 pressure transducer located closest to the exit of the channel. Test32 and Tests34 were performed in the channel with four obstacles and a hydrogen mixture with ER = 0.6. The pressure development is similar to that of Test09 and Test47 with two obstacles. However, for ER = 0.6 the s_{QL} predictions by both versions are alike and the initial flame propagation is similar.

Fig. 9 shows the maximum overpressure inside the channel as a function of the equivalence ratio for the tests with two obstacles (a) and for the tests with four obstacles (b). Both FLACS-CFD versions capture the trends of maximum overpressure with equivalence ratio observed in the experiments. The predicted overpressures by FLACS-CFD *22.1 IH* for the two geometry configurations are within a factor of 2 of the values observed in the experiments for lean hydrogen-air mixtures, for rich hydrogen-air mixtures, the overprediction increases with the equivalence ratio.

4.4. HySEA

Fig. 10 shows the pressure-time curves for the two scenarios with repetitions (8 or 6 m² vent area covered by commercial vent panels). The pressure-time curves were filtered using a 50 Hz filter. The grid resolution is 0.1 m. The maximum overpressure was similar at the different sensors and only P4 is shown in the figure.

The pressure starts increasing slowly until the flame moves through the first row of pipes. In this phase, the flame propagation is governed by
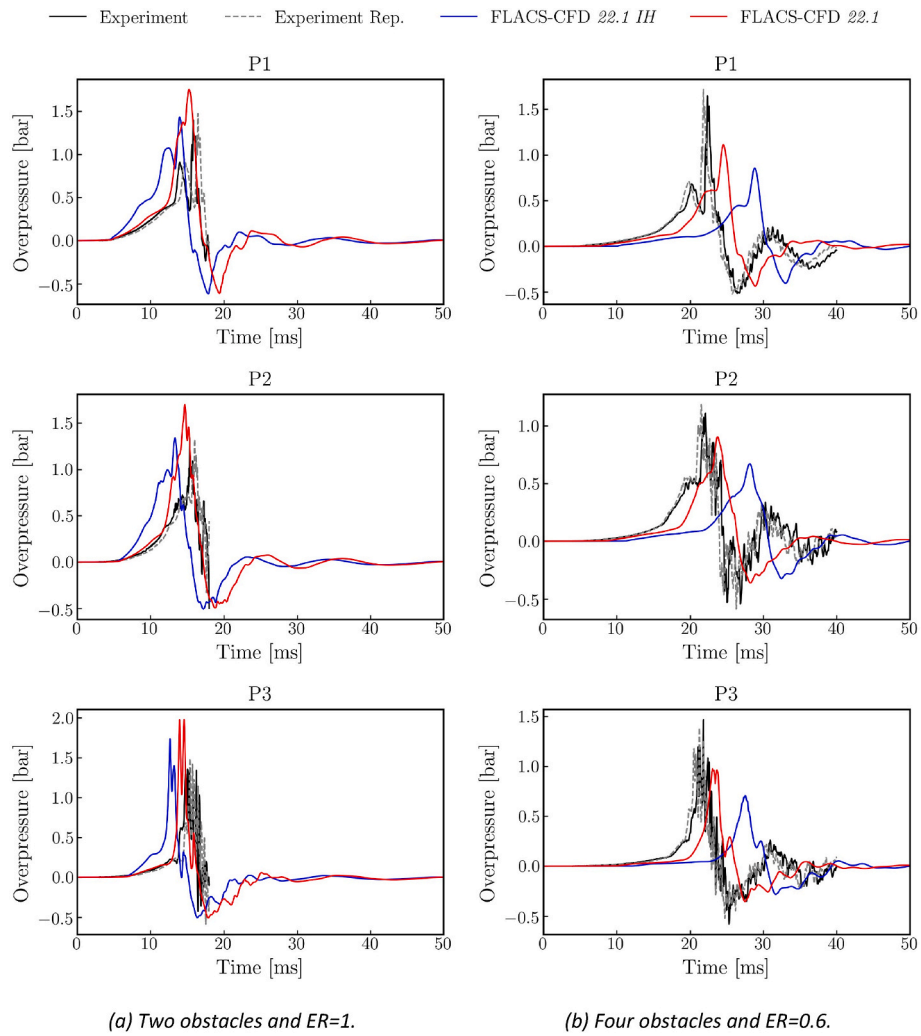
(a) Two obstacles and ER=1.   *(b) Four obstacles and ER=0.6.*

Fig. 8. Pressure-time curves for the tests in MOGELEG channel.

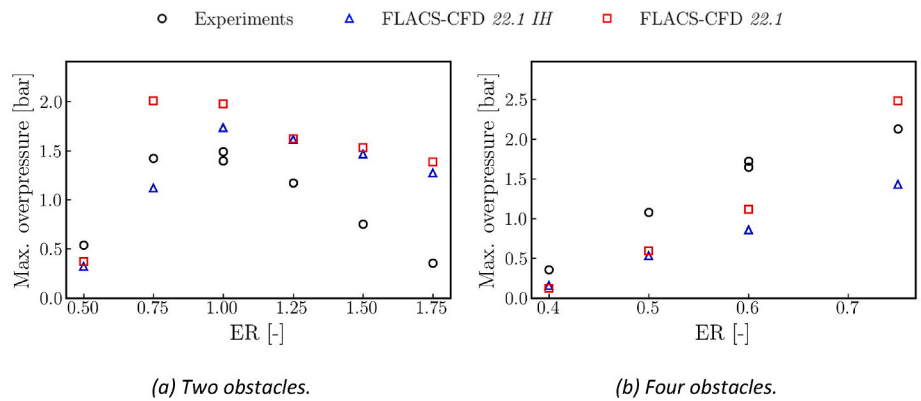
(a) Two obstacles.   *(b) Four obstacles.*

Fig. 9. Maximum overpressure with equivalence ratio for the MOGELEG experiments with hydrogen.

the quasi-laminar regime. The flame propagation is faster in the FLACS-CFD *22.1* than in the FLACS-CFD *22.1 IH* predictions because of the higher laminar burning velocity used in the quasi-laminar burning velocity model. When the flame passes through the obstacles, the turbulent regime dominates. The maximum overpressure occurs when the flame reaches the vent opening. Fig. 11 shows the predicted versus the measured maximum overpressure for the HySEA experiments in a scatter plot. Each point corresponds to a pressure transducer for a given

test. The overall overpredictions of the peak overpressures are considerably reduced using the FLACS-CFD *22.1 IH* instead of the FLACS-CFD *22.1* version. The FLACS-CFD *22.1 IH* predictions that do not fall within a factor of 2 correspond to the tests with commercial vent panels. The predictions are quite sensitive to the modelling of the panels and overprediction in those scenarios may be related to the representation of the opening of the panels (Skjold et al., 2019).

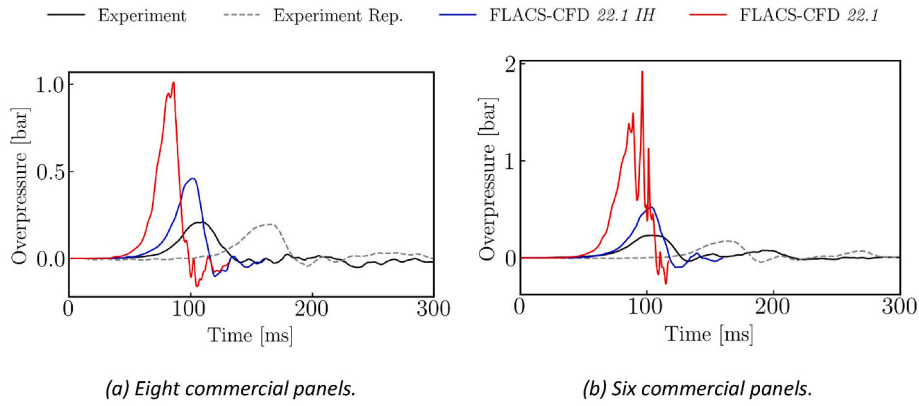The severe overpredictions in FLACS-CFD *22.1* seem to be related to

(a) Eight commercial panels.   (b) Six commercial panels.

Fig. 10. Pressure-time curves at pressure transducer P4 for the HySEA experiments.
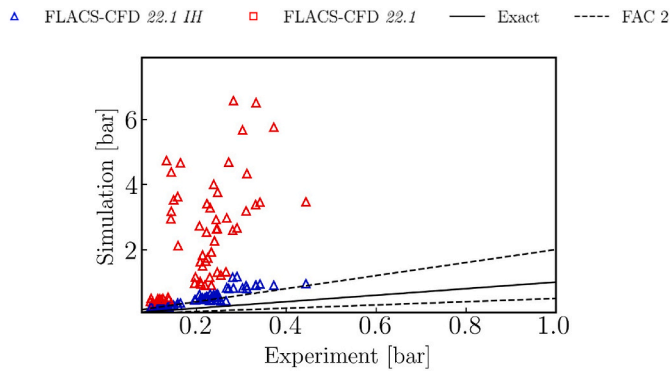

Fig. 11. Scatter plot of maximum overpressure at each sensor for the HySEA experiments.

the Lewis correction applied to the laminar burning velocity that enhances the burning velocity in all regimes for the equivalence ratios used in these experiments.

4.5. Repeated pipe congestion

Fig. 12a compares the maximum overpressure observed in the hydrogen experiments with the predicted maximum overpressure by FLACS-CFD *22.1* and FLACS-CFD *22.1 IH* for different equivalence ratios. The grid resolution is 0.133 m. The highest maximum overpressure in the experiments occurs for the mixture with ER = 1.253 and the lowest maximum overpressure is observed for the lean mixture with an ER of 0.8. FLACS-CFD *22.1 IH* predicts the maximum overpressure at ER = 1.25, as observed in the experiments. However, FLACS-CFD *22.1*

predicts the highest overpressure at ER = 0.97. The laminar burning velocity in FLACS-CFD *22.1* is higher at ER = 0.97 than at ER = 1.25 due to the Lewis number correction applied. The predicted overpressure for lean hydrogen mixtures is lower with FLACS-CFD *22.1 IH* than with FLACS-CFD *22.1*. For the richest mixture (ER = 1.8), neither version capture the significant reduction in overpressure compared to the near-stoichiometric mixtures. At ER = 1.8 the maximum simulated overpressure is about 1.5 higher than the observed overpressure. Fig. 12b compares the maximum overpressure observed in the experiments with the predicted maximum overpressure by FLACS-CFD *22.1* and FLACS-CFD *22.1 IH* for different hydrogen concentrations (in hydrogen-methane blends). The maximum overpressure increases with the hydrogen concentration. The increase in maximum overpressure is more pronounced for the predictions by FLACS-CFD *22.1 IH* than for experiments and FLACS-CFD *22.1*. This can be explained by the differences in the laminar burning velocity. As shown by the green plus symbols in Fig. 12b, the predictions by FLACS-CFD *22.1 IH* with s_L obtained from Cantera using the GRI-Mech 3.0 mechanism shows a better fit with the experimental trends of overpressure with hydrogen content.

4.6. Overall discussion

In general, the maximum overpressure predictions by FLACS-CFD *22.1 IH* as a function of the ER follow the trends of s_L with ER (Fig. 13a) for all the scenarios in this paper. For the experimental measurements and the FLACS-CFD *22.1 IH* predictions, the maximum overpressures occur for mixtures slightly richer than at stoichiometric conditions. For FLACS-CFD *22.1*, the highest overpressure is predicted for lean mixtures. Fig. 13b shows s_L as a function of the hydrogen concentration for hydrogen-methane blends with an ER = 1.1 and ambient pressure and temperature. The values used in FLACS-CFD differ from the values computed using the one-dimensional detailed chemistry flame
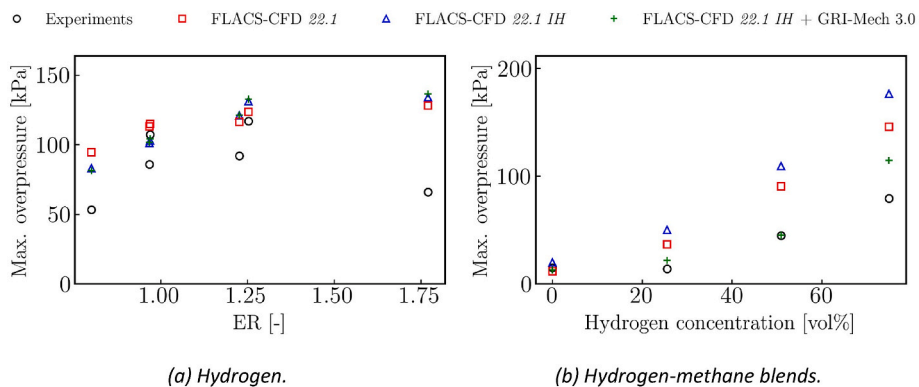

(a) Hydrogen.   (b) Hydrogen-methane blends.

Fig. 12. Maximum overpressure trends for the repeated pipe congestion experiments.
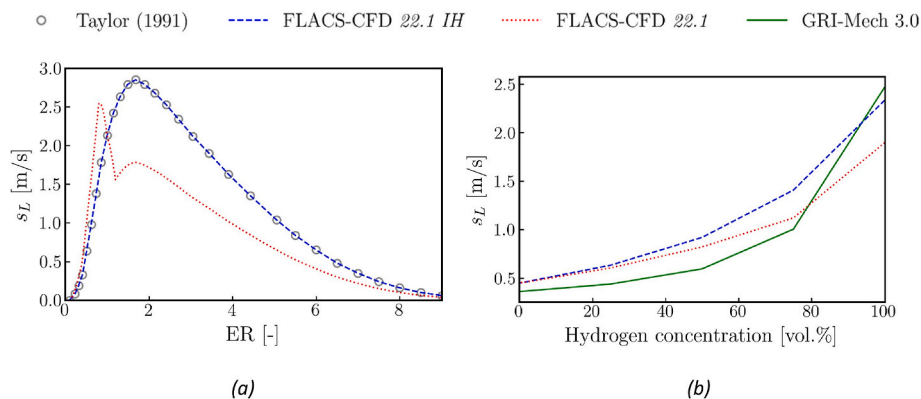
Fig. 13. s_L vs. ER for 100% hydrogen mixtures (a) and s_L vs. hydrogen concentration for hydrogen-methane blends (b).

solver with the GRI-Mech 3.0 mechanism. The maximum difference between FLACS-CFD *22.1 IH* and the GRI-Mech 3.0 values is about 54%. The uncertainty in measuring s_L for hydrogen-air can reach $\pm50\%$ for ER < 0.5, $\pm20\%$ for ER > 3 and $\pm10\%$ for $1 < \text{ER} < 3$ according to Han et al. (2020). A sensitivity study for the input s_L was performed for the hydrogen-methane tests in the repeated pipe congestion geometry. As shown by the error bars in Fig. 14, modifying s_L by 20% results in up to an 80% variation in maximum overpressure in these scenarios. This implies that more accurate values of s_L can improve the predictions for hydrogen-methane blends. To the authors' knowledge, there are not available mechanisms to be used in one-dimensional detailed reaction mechanism tools that include all the compounds that are available in FLACS-CFD. Therefore, using the s_L computed directly from these kinds of tools is a limitation for the number of blends to be simulated. Bradley et al. (2017) showed the comparison of well-known mixture rules with experimental data and proposed a new rule that seems to estimate better the s_L for hydrogen-methane blends. Mixture rules for Markstein lengths were also investigated, although the calculated values were less accurate than the measurements maximum uncertainty. However, as shown in Fig. 14, a variation of only about 13% in maximum overpressure is observed when varying the Ma_{sr} by $\pm60\%$. The Ma_{sr} numbers used in Equation (4) are obtained from stationary spherical flames and spherical implosion computations (Bradley et al., 1996). However, the Markstein number, accounting for both curvature and strain effects, is reported by most experimental (Hu et al., 2009; Han et al., 2020; Kwon, 2004) and computational (Ruiz et al., 2021; Maxwell et al., 2021) studies on the laminar burning velocity for hydrogen and hydrogen blends. Correlations similar to the expressions in Equation (4) as a function of the Markstein length should be explored.
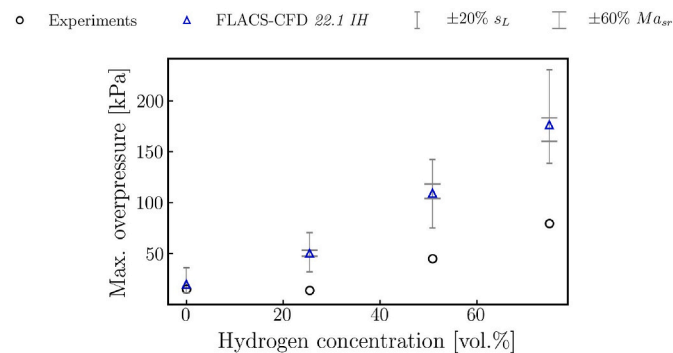
5. Conclusions

A set of simulation results for experimental campaigns for evaluating the validity of the burning velocity models used in advanced consequence tools has been presented. The performance of two versions of the CFD tool FLACS, FLACS-CFD *22.1* and FLACS-CFD *22.1 IH*, has been evaluated. The FLACS-CFD *22.1 IH* predictions of the maximum overpressure in this paper are in better agreement with the experiments than the predictions by FLACS-CFD *22.1*. Except for the HySEA experiments, the predictions by FLACS-CFD *22.1 IH* for lean hydrogen mixtures are within a factor 2 of the values observed in the experiments. Repeated experiments of large scale realistic scenarios have shown a variation of a factor of 2 on the predicted overpressures (Skjold et al., 2022), therefore this is considered as an acceptable prediction. Improvements of the model are needed for more accurate prediction of deflagrations of rich hydrogen mixtures. FLACS-CFD *22.1 IH* uses empirical correlations expressed in terms of the Markstein strain number to compute the turbulent burning velocities. Although the model predicts the maximum overpressure trends observed in the experiments with better accuracy than FLACS-CFD *22.1*, the model has important limitations. The correlations were implemented to be valid only for initially atmospheric pressures and standard ambient temperatures, and for mixtures of hydrogen with air (no added inerts). For mixtures with other fuels, a simple volume fraction-weighted approach was used. There is no available data for all fuels in the literature and the correlations used here might not be equally valid for other fuels or pressure and temperature conditions. Most of the measurements available in the literature report the Markstein number directly, that accounts for both strain and curvature effects. Thus, further work should focus on studying the possibility of an expression for α and β as a function of the Markstein number. The Markstein number datasets might be computed from one-dimensional detailed chemistry flame solvers such as CosiLab or Cantera. New mixture rules and correlations for pressure and temperature might be needed.

Author statement

Melodia Lucas: Software, Formal analysis, Data Curation, Visualization, Validation, Writing-Original draft preparation. **Helene Hisken:** Supervision, Writing - Review & Editing, Resources, Conceptualization. **Kees van Wingerden:** Supervision, Writing - Review & Editing. **Bjørn J. Artzen:** Supervision, Writing - Review & Editing. **Trygve Skjold:** Supervision, Writing - Review & Editing, Resources.

Declaration of competing interest

The authors declare that they have no known competing financial interests or personal relationships that could have appeared to influence the work reported in this paper.

Fig. 14. s_L and Ma_{sr} uncertainty effects in the hydrogen-methane blend tests in the repeated pipe congestion.

Data availability

The authors do not have permission to share data.

Acknowledgements

References

Bauwens, C., Bergthorson, J., Dorofeev, S., 2017a. Experimental investigation of spherical-flame acceleration in lean hydrogen-air mixtures. Int. J. Hydrogen Energy 42 (11), 7691–7697.

Bauwens, C., Bergthorson, J., Dorofeev, S., 2017b. On the interaction of the Darrieus–Landau instability with weak initial turbulence. Proc. Combust. Inst. 36 (2), 2815–2822.

Bauwens, C., Chao, J., Dorofeev, S., 2012. Effect of hydrogen concentration on vented explosion overpressures from lean hydrogen-air deflagrations. Int. J. Hydrogen Energy 37 (22), 17599–17605.

Both, A.-L., Gordon, A., Hisken, H., 2019. CFD modelling of gas explosions: optimising sub-grid model parameters. J. Loss Prev. Process. Ind. 60, 159–173.

Bradley, D., Gaskell, P., Gu, X., 1996. Burning velocities, Markstein lengths, and flame quenching for spherical methane-air flames: a computational study. Combust. Flame 104 (1–2), 176–198.

Bradley, D., Lawes, M., Liu, K., Mansour, M., 2013. Measurements and correlations of turbulent burning velocities over wide ranges of fuels and elevated pressures. Proc. Combust. Inst. 34 (1), 1519–1526.

Bradley, D., Lawes, M., Mumby, R., 2017. Burning velocity and Markstein length blending laws for methane/air and hydrogen/air blends. Fuel 187, 268–275.

Bray, K., 1990. Studies of the turbulent burning velocity. Proc. Math. Phys. Sci. 431, 315–335, 1882.

Breitung, W., Dorofeev, S.A., Kotchourko, A., Redlinger, R., Scholtyssek, W., Bentaib, A., Heriteau, J.-P., Pailhories, P., Eyink, J., Movahed, M., Petzold, K.-G., Heitsch, M., Alekseev, V., Denkevits, A., Efimenko, A., Okun, M., Huld, T., Baraldi, D., 2005. Integral large scale experiments on hydrogen combustion for severe accident code validation-HYCOM. Nucl. Eng. Des. 235, 253–270.

Gexcon, A.S., 2022. FLACS-CFD v22.1 User Manual. Technical Report, Gexcon AS, Bergen, Norway.

Han, W., Dai, P., Gou, X., Chen, Z., 2020. A review of laminar flame speeds of hydrogen and syngas measured from propagating spherical flames. Applications in Energy and Combustion Science 1, 100008.

Hisken, H., 2018. Investigation of Instability and Turbulence Effects on Gas Explosions: Experiments and Modelling. Ph.D. thesis, University of Bergen.

Hu, E., Huang, Z., He, J., Jin, C., Zheng, J., 2009. Experimental and numerical study on laminar burning characteristics of premixed methane–hydrogen–air flames. Int. J. Hydrogen Energy 34 (11), 4876–4888.

Kwon, O., 2004. Dynamic properties of outwardly propagating spherical hydrogen-air flames at high temperatures and pressures. KSME Int. J. 18 (2), 325–334.

Launder, B.E., Spalding, D.B., 1974. The numerical computation of turbulent flows. Comput. Methods Appl. Mech. Eng. 3 (2).

Lucas, M., Atanga, G., Hisken, H., Mauri, L., Skjold, T., 2021. Simulating vented hydrogen deflagrations: improved modelling in the CFD tool FLACS-hydrogen. Int. J. Hydrogen Energy 46 (23), 12464–12473..

Makarov, D., Verbecke, F., Molkov, V., Roe, O., Skotenne, M., Kotchourko, A., Lelyakin, A., Yanez, J., Hansen, O., Middha, P., Ledin, S., Baraldi, D., Heitsch, M., Efimenko, A., Gavrikov, A., 2009. An inter-comparison exercise on cfd model capabilities to predict a hydrogen explosion in a simulated vehicle refuelling environment. Int. J. Hydrogen Energy 34 (6), 2800–2814..

Maxwell, B., Mével, R., Melguizo-Gavilanes, J., 2021. Spherically expanding flame simulations in Cantera using a Lagrangian formulation. ICHS 2021, Ediburgh, Scotland.

Middha, P., 2010. Development, Use, and Validation of the CFD Tool FLACS for Hydrogen Safety Studies. Ph.D. thesis, Department of Physics and Technology, University of Bergen.

Middha, P., Hansen, O., Groethe, M., Arntzen, B., 2007. Hydrogen explosion study in a confined tube: FLACS CFD simulations and experiments. In: Twenty-first International Colloquium of Dynamics of Explosions and Reactive Systems. Poitiers, France.

Muthusamy, D., Hansen, O., Middha, P., Royle, M., Willoughby, D., 2011. Modelling of Hydrogen Jet Fires Using CFD. ICHS 2011, San Francisco, CA, USA.

Renoult, J., Wilkins, B., 2004. Hydrogen explosion safety phase 2 - small scale explosion experiments. Technical report, Gexcon AS.

Royle, M., Shirvill, L., Roberts, T., 2007. Vapour Cloud explosions from the ignition of methane/hydrogen/air mixtures in a congested region. ICHS 2007, San Sebastian, Spain.

Ruiz, F., Beardsell, G., Blanquart, G., 2021. Framework for simulating stationary spherical flames. Proc. Combust. Inst. 38 (2), 2109–2117.

Sato, Y., Merilo, E., Groethe, M., Colton, J., Chiba, S., Iwabuchi, H., 2006. Homogeneous hydrogen deflagrations in a sub-scale vehicle tunnel. National Hydrogen Association Annual hydrogen Conference, Long Beech, CA, USA.

Shirvill, L.C., Roberts, T.A., Royle, M., Willoughby, D.B., Sathiah, P., 2019a. Experimental study of hydrogen explosion in repeated pipe congestion – part 1: effects of increase in congestion. Int. J. Hydrogen Energy 44, 9466–9483.

Shirvill, L.C., Roberts, T.A., Royle, M., Willoughby, D.B., Sathiah, P., 2019b. Experimental study of hydrogen explosion in repeated pipe congestion – Part 2: effects of increase in hydrogen concentration in hydrogen-methane-air mixture. Int. J. Hydrogen Energy 44 (5), 3264–3276.

Skjold, T., 2018. Vented Hydrogen Deflagrations in 20-foot ISO Containers. In: Proceedings of the Twelfth International Symposium on Hazards, Prevention and Mitigation of Industrial Explosions (XII ISHPMIE), Kansas City, MO, USA, pp. 823–846.

Skjold, T., 2020. On the Strength of Knowledge in Risk Assessments for Hydrogen Systems. In: Proceedings of the Thirteenth International Symposium on Hazards. Prevention and Mitigation of Industrial Explosions (ISHPMIE2020).

Skjold, T., Hisken, H., Bernard, L., Mauri, L., Atanga, G., Lakshmipathy, S., Melodia, L., Carcassi, M., Schiavetti, M., Rao, V., Sinha, A., Wen, J., Tolias, I., Giannissi, S., Venetsanos, A., Stewart, J., Hansen, O., Kumar, G., Krumenacker, L., Laviron, F., Jambut, R., Huser, A., 2019. Blindprediction: estimating the consequences of vented hydrogen deflagrations for inhomogeneous mixtures in 20-foot ISO containers. J. Loss Prev. Process. Ind. 61, 220–236.

Skjold, T., Hisken, H., Derempouka, E., Lucas, M., Johnson, D., 2022. Strength of knowledge in risk assessments for fuel-air explosions in complex geometries: implications for hydrogen systems. In: Proceedings of the Tenth International Seminar on Fire and Explosion Hazards(ISFEH10), Oslo, Norway.

Skjold, T., Hisken, H., Lakshmipathy, S., Atanga, G., van Wingerden, M., Olsen, K.L., Holme, M., Turøy, N., van Wingerden, K., 2017. Experimental Investigation of Vented Hydrogen Deflagrations in Containers. Phase 1: Homogeneous Mixtures. Technical report, Report HySEA-D2-04-2017.

Taylor, S.C., 1991. Burning Velocity and the Influence of Flame Stretch. Ph.D. thesis, University of Leeds, UK.